Journal of Nuclear Materials 400 (2010) 25–31

Contents lists available at ScienceDirect

Journal of Nuclear Materials

journal homepage: www.elsevier.com/locate/jnucmat

Functionalized porous glass for the removal and the confinement of ruthenium from radioactive solutions

Alexei Tokarev [a], Agnès Grandjean [b,*], Yannick Guari [a,*], Joulia Larionova [a], Rachel Pflieger [b], Christian Guérin [a]

[a] Institut Charles Gerhardt Montpellier, UMR 5253 CNRS-UM2-ENSCM-UM1, Chimie Moléculaire et Organisation du Solide, Université Montpellier II, Place E. Bataillon, 34095 Montpellier Cedex 5, France
[b] Institut de Chimie Séparative de Marcoule, UMR5257 CEA-CNRS-UM2-ENSCM, 30207 Bagnols sur Cèze, France

ARTICLE INFO

Article history:
Received 23 October 2009
Accepted 5 February 2010

ABSTRACT

An original approach to immobilize ruthenium species and then transform them into RuO_2 nanoparticles is presented that uses hybrid-functionalized glasses. First, different chemical graftings of functional groups (acetylacetonate, amine, nitrile, pyridine and thiol) in porous glass were used to extract ruthenium-containing complexes ($[Ru(CH_3N)_4Cl_2]$ and $Ru(NO)(NO_3)_3$) from solutions. The best functional groups to selectively coordinate Ru complexes and thus extract it from the solutions have been determined. Then, the obtained Ru-containing composite glass was heated under air to remove the organic species and to obtain RuO_2 nanoparticles inside a glass with centimetre scale geometric form. The as-obtained materials were studied by transmission electron microscopy (TEM), scanning electron microscopy (SEM), nitrogen physisorbtion measurements, elemental analysis and X-ray diffraction (XRD).

1. Introduction

Environmental impact of the release of toxic and radioactive pollutants from nuclear industry has led to a wide variety of studies on the removal of such pollutants. In the reprocessing step of spent nuclear fuel, uranium and plutonium are quantitatively recovered from the solution of spent fuel in nitric acid, leaving radioactive fission products inside the nitric acid solution. This solution containing fission products is referred to as high level radioactive liquid waste (HLW). Moreover low-level radioactive waste (LLW) and also intermediate level radioactive liquid waste (ILW) solutions are generated in large volumes mainly in spent fuel reprocessing plants.

All these waste streams are contaminated with fission products produced by the ^{235}U and ^{239}Pu and ^{241}Pu fission processes. Different radionuclides of about 40 elements have been observed in these solutions including those of ruthenium. These waste solutions are eventually solidified, stored and disposed for example as vitrified materials. Generally, ruthenium is one of the most troublesome elements for at least three major reasons. First ruthenium exhibits multiple oxidation states (zero, II, III, IV, VI, VIII), a complex chemistry, and seven isotopes produced during the fission reaction: ^{99}Ru (stable), ^{101}Ru (stable), ^{102}Ru (stable), ^{103}Ru ($T_{1/2}$ = 39.27 d), ^{104}Ru (stable), ^{105}Ru ($T_{1/2}$ = 4.44 h), ^{106}Ru ($T_{1/2}$ = 1.02 y). Secondly, it can easily transfer into various ecosystems [1]. Thirdly, when the high level liquid waste is melt mixed with a vitrifying agent in a melting furnace, the platinum group metals, and especially ruthenium, are the major fission products which interfere with a stable operation of the glass melting process. Indeed, during the dissolution of the HLW into the molten glass, these metals whose solubility is very low in the molten glass, are partially precipitated and accumulate at the bottom of the melter [2]. Formation of a conductive metallic sludge may cause a serious loss of electrical current in the glass in case of joule heating melter, that may cause erosion of the melter and shorten its lifetime [3]. Moreover the oxygen fugacity of a given high level waste vitrification facility can be problematic when RuO_2 is present. In case of electrode melter, if it is operated highly reducing, the Ru can precipitate as metallic Ru and short out the electrodes as can also do RuO_2 if present in enough quantity [4–6].

On the other hand, ruthenium-106 and -103 have important applications in nuclear medicine: ^{106}Ru is used as an external irradiator for treatment of benign conditions of eye and in preparation for corneal transplant [7]; ruthenium 103 is used for myocardial blood flow and positron emission tomography imaging [8]. For these reasons, the selective recuperation of the Ru species from the radioactive liquid waste can present increasing interest and different approaches have been proposed: e.g. solvent extraction of promethium(III), uranium(VI), plutonium(IV), americium(III), zirconium(IV), ruthenium(III), iron(III) and palladium(II) with a

* Corresponding authors. Tel.: +33 4 66 79 66 22 (A. Grandjean).
E-mail addresses: agnes.grandjean@cea.fr (A. Grandjean), yannick.guari@univ-montp2.fr (Y. Guari).

0022-3115/$ - see front matter © 2010 Elsevier B.V. All rights reserved.
doi:10.1016/j.jnucmat.2010.02.005

mixture of octyl(phenyl)-N,N-diisobutylcarbamoylmethylphosphine oxide (CMPO) and tributyl phosphate (TBP) in dodecane [9], ion exchange methods [10,11], co-precipitation methods [12,13], and distillation and precipitation [7,8].

Several materials like clays, zeolites, nafion, and polymeric resin have been studied for the removal of environmentally hazardous materials including radionuclides based on various methodologies such as preconcentration and molecular recognition/discrimination, as well as electrochemistry (ion exchange voltammetry, indirect amperometric detection, and potentiometry). Until now, there have been only few studies devoted to the design of ordered mesoporous silica-based functionalized materials possessing ion exchange properties that would be devoted to waste immobilization. Functional groups carried on the mesopores surface of silica-based materials allow specific interaction with various compounds. In case of ruthenium, the removal of residual ruthenium after olefin metathesis reactions and asymmetric hydrogenations has been described using amine-functionalized mesoporous silicates [14]. But in the case of nuclear waste management, there are only few examples of using functionalized mesoporous materials. For example, several mesoporous titanium phosphate phases, with varying pore sizes, were prepared using non-ionic surfactants and these materials were shown to have high affinity for certain radionuclides [15].

Because the ratio of Ru to HLW increases with increasing burn up (that is expected to increase in the future), the aims of this work is to propose a new prospective way for the separation and the confinement of Ru species from nuclear waste solutions. Our approach consists in using hybrid porous glasses functionalized with organic groups. These hybrid glasses prepared by controlled crystallization of glass, using spinodal-type phase separation, subsequent acid treatment (Vycor process) and post synthetic functionalization present several advantages: (i) they have a very flexible geometric form, pores size in the range from 1 nm to 1000 nm and a very reactive surface [16]; (ii) in comparison to the other materials (such as polymers, glasses produced by the sol–gel method) they present excellent thermal and chemical durability, mechanical strength, and irradiation damage resistance in combination with controlled structural characteristics [17]; (iii) they present organic functionalities able to coordinate Ru complexes.

Here we present an original approach in order to immobilize ruthenium species and to get their transform ion into RuO_2 nanoparticles by using hybrid-functionalized glasses. First, different chemical graftings of functional groups (acetylacetonate, amine, nitrile, pyridine and thiol) in porous glass were used to extract ruthenium-containing complexes ($[Ru(CH_3N)_4Cl_2]$ and $Ru(NO)(NO_3)_3$) from solutions. The best functional groups to selectively coordinate Ru complexes and thus extract it from the solutions have been determined. Then, the obtained Ru-containing composite glass was heated under air to remove the organic species and to obtain RuO_2 nanoparticles inside a glass with centimetre scale geometric form.

2. Experimental part

All the chemical reagents were of analytical grade. Elemental analyses were performed by the Service Central d'Analyse (CNRS, Vernaison, France). The samples were heated at 3000 °C under He. Oxygen was transformed into CO and detected by an IR detector. Ruthenium, silicon, sodium and boron were determined with a high resolution ICP–MS using a ThermoFischer element. Here the detection limit is evaluated lower then 10 ppm and the uncertainty lower than 2%.

An evaluation of the Ru/Si ratio was also performed by using an Environmental Secondary Electron Microscope FEI Quanta 200 FEG coupled with an Electrons Dispersive Spectroscope Oxford INCA detector. Using this analytical method, the uncertainty is evaluated to 10%.

2.1. Synthesis of base porous glass

Silica, orthoboric acid, and sodium carbonate powders were used to prepare the primitive glass samples. The glass composition 75 mol% SiO_2, 5 mol% Na_2O and 20 mol% B_2O_3 was used here, which can exhibit spinodal phase separation. SiO_2 and Na_2CO_3 powders were dried for 24 h at 1000 °C (350 °C for Na_2CO_3) whereas H_3BO_3 was used in its as-received form. First the chemicals were thoroughly mixed. Then the mixtures were slowly heated in Pt–Au crucibles to decompose the borate, carbonate or nitrate components, and then melted for 4.5 h at 1350 °C. The melt was cooled at a rate of 300 °C/h until 550 °C and then annealed at 550 °C during 10 h. Then the sample was quenched quickly. Once cooled, the sample was taken out of the crucible. The glass sample was then ground to powder, etched with an aqueous solution of 3 M HCl at 90 °C during 24 h, and washed with water and dried in an air oven at 120 °C. Analyses of the sample composition are given in Table 1.

2.2. Grafting of porous glasses

The grafting of various organic functionalities into the silica pores was performed by refluxing in toluene over night the base porous glass in the presence of the respective organic precursors $(CH_3O)_3Si(CH_2)_nR$ (R = SH (**a**), C_5H_4N (**b**), NH_2 (**c**), CN (**d**), acac (**e**)) (Fig. 1), where $n = 2$ or 3 [18]. Precursors (**a**), (**c**) and (**d**) were obtained from commercial sources while (**b**) and (**e**) were synthesized by using previously published procedures [19,20]. Typical procedure was to dry under vacuum 3 g of milled glass in round bottom flask, then to add 100 mL of preliminarily distilled toluene. Then 1 mL ((**a**), 5.38 mmol; (**b**), 4.66 mmol; (**c**), 4.25 mmol; (**d**), 4.17 mmol; (**e**), 3.12 mmol) of the organic precursor was added under argon and the suspension was heated at reflux for 24 h. The solvent was removed by filtration and the functionalized glass was washed in toluene, ethanol and acetone. The residue of solvents was eliminated in a vacuum oven at 120 °C for 4–5 h. Analyses of the samples composition are given on Table 1.

2.3. Extraction of Ru ions from solutions by functionalized porous glasses

The incorporation of the Ru ions or complexes into the functionalized porous glasses **1a–e** were performed for two distinct Ru-containing complexes, $[Ru(CH_3CN)_4Cl_2]$ [21] and $Ru(NO_3)_3(NO)$ with pH = 7. These complexes are shown in Fig. 2.

Table 1
Elemental analyses of the base glass **1** and of the composite glasses $R(CH_2)_nSiO_{1.5}/SiO_2–Na_2O–B_2O_3$ **1a–e**.

Material	SiO_2	B_2O_3	Na_2O	$R(CH_2)_nSiO_{1.5}$	
	(moles%)	(moles%)	(moles%)	(moles%)	(mmol g^{-1})
1	90.9	8.3	0.8	–	0.084–0.139[a]
1a	90.1	8.5	0.8	0.6	0.090
1b	90.2	8.1	0.7	1.0	0.164
1c	89.5	8.6	0.7	1.2	0.198
1d	89.8	8.2	0.8	1.2	0.188
1e	90.6	8.6	0.8	–	–

[a] Estimation of available free sites.

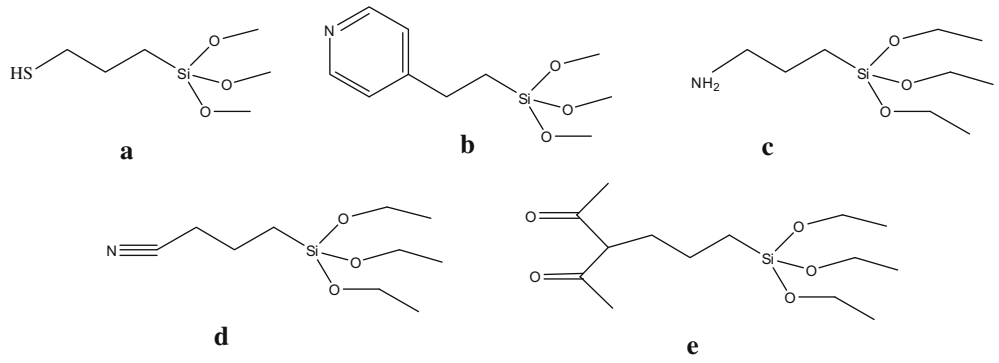

Fig. 1. Organic precursors a–e used for the grafting of porous glasses.

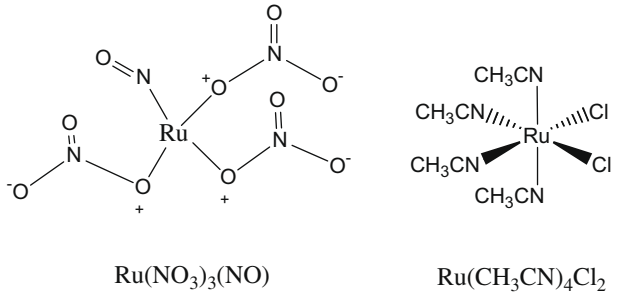

Fig. 2. Ruthenium complexes used.

The extraction was performed using the following procedure. Hybrid glass powder of **1a–e** (75 mg) was added to a 10^{-2} M (10 mL) solution of the complex in water. The mixture was stirred overnight at room temperature. After filtration, the powder was thoroughly washed several times with water and methanol and dried at room temperature *in vaccum* for 24 h. These samples are called **2a–e** for the $[Ru(CH_3CN)_4Cl_2]$ complex and **3a–e** for the $Ru(NO_3)_3(NO)$ complex. The selectivity checked of the $[Ru(CH_3CN)_4Cl_2]$ extraction in the presence of Er^{3+} ions by the functionalized glass **1a** was performed in the same manner by using 10^{-2} M mixed solution of $[Ru(CH_3CN)_4Cl_2]$ and $ErCl_3$. Analyses of the samples composition are given on Table 3. For complexes **3a–e**, the amount of Ru was <0.05 wt.%.

2.4. Calcination of composite 2a and formation of RuO_2 nanoparticles

Composite **2a** has been calcined under air up to 650 °C. The obtained composite is called **4a**.

Table 2
Some relevant characteristics of the base glass **1** and grafted hybrid glasses $R(CH_2)_nSiO_{1.5}/SiO_2–Na_2O–B_2O_3$ **1a–e**.

Material	R-group	Specific pore volume, $m^3\ g^{-1}$	Specific surface area, $m^2\ g^{-1}$
1	–	0.11 ± 0.01	42
1a	SH	0.11 ± 0.01	33
1b	C_5H_4N	0.04 ± 0.01	8
1c	NH_2	0.09 ± 0.01	19
1d	CN	0.08 ± 0.01	30
1e	acac	0.11 ± 0.01	36

Table 3
Elemental analyses of the composite glasses **2a–e** obtained after incorporation of the $[Ru^{II}(CH_3CN)_4Cl_2]$ complex. Yield corresponds to the ratio Ru extracted (moles) to the functionalized group.

Material	SiO_2	B_2O_3	Na_2O	$R(CH_2)_n$	RuO_2	"yield"
	(moles%)	(moles%)	(moles%)	(moles%)	(moles%)	%
2a	90.9	8.2	0.9	0.7	0.4	57
2b	89.3	7.9	0.9	1.6	0.3	18
2c	90.1	7.6	0.8	1.4	0.2	14
2d	89.3	8.0	0.9	1.7	0.1	6
2e	91.7	7.4	0.8	_	0.1	_

2.4.1. Physical measurements

IR spectra were recorded on a Perkin Elmer 1600 spectrometer with 4 cm^{-1} resolution. UV–Vis spectra were recorded in KBr disks on a Cary 5E spectrometer. X-ray diffraction patterns were measured on a PanAnalytical diffractometer equipped with an ultra-fast X'celerator detector X'pert Pro with nickel-filtered copper radiation (1.5405 Å). A 92–16.18 SETARAM TG analyser was employed in air for the measurement of the mass loss of the samples *via* thermal gravimetric analysis (TGA), with a relative uncertainty of ±5 K at 600 °C. The heating slope used for these analyses was fixed to 10 °C/min. After etched with the aqueous solution of 3 M HCl,, some glass pellets were polished and characterized by scanning electron microscopy SEM. Samples for transmission electron microscopy (TEM) measurements were prepared using ultramicrotomy techniques and then deposited on copper grids. TEM measurements were carried out at 100 kV with a JEOL 1200 EXII microscope. Specific surface areas were determined by the Brunauer–Emmett–Teller (BET) method with TriStar 3000 V6.06 A analyser. Prior to the measurement, samples were evacuated at 120 °C during 12 h. The pore-size distribution was calculated using the Barrett–Joyner–Halenda (BJH) method. It should be noted that this well-established theory is an appropriate method for the determination of the pore-size distribution of materials with pores larger than 4 nm.

3. Results and discussion

Fig. 3 represents the approach we considered to extract Ru complexes from solutions by using hybrid-functionalized porous glasses and to transform them into ruthenium dioxide nanoparticles. The first step consists in the chemical anchorage of the appropriate organic functionality into the pores of glass. The second one is the coordination of this functionality to the Ru-containing complex in order to selectively extract this compound from aqueous solution. Different organic functionalities as well as different Ru-containing complexes have been used in this study in order to

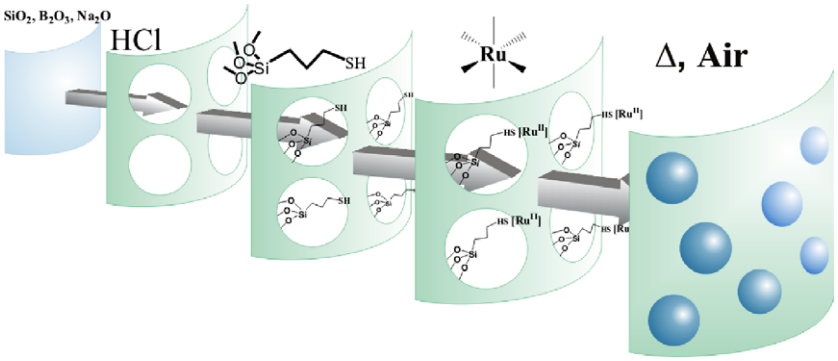

Fig. 3. Schematic representation of the ruthenium complex extraction and subsequent preparation of RuO_2 nanoparticles inserted within the glass matrix.

determine "the best" organic group to extract Ru complexes from aqueous solutions. The third step consists in the transformation *via* thermal treatment of Ru-containing composite glasses into the nanocomposite materials containing RuO_2 nanoparticles. The different physical characterisations allowed us to monitor the evolution of our material at each step of its synthesis.

3.1. Synthesis and characterisation of base and functionalized hybrid glasses

3.1.1. Base glass

The synthesis of the porous base glass was performed by controlled crystallization of glass, using spinodal-type phase separation and subsequent acid treatment (Vycor process, see Section 2). The amorphous behaviour of the sample was checked using X-ray diffraction analysis. Analysis by ICP/MS gave a composition of 90.9 SiO_2-0.8 Na_2O-8.3 B_2O_3 (Table 1).

The porous texture of the base glass was determined using nitrogen adsorption at boiling temperature (77 K) (see Section 2). As shown Fig. 4, this sample is characterized by a large amount of adsorption at low relative pressure, a nearly horizontal plateau and a hysteresis between the adsorption curve and the desorption one's. This behaviour means that this sample presents micro and mesoporosities. According to IUPAC classification, four types of hysteresis have been distinguished [22]. In our case, mesoporous samples exhibit a H2 type hysteresis. This type is characteristics

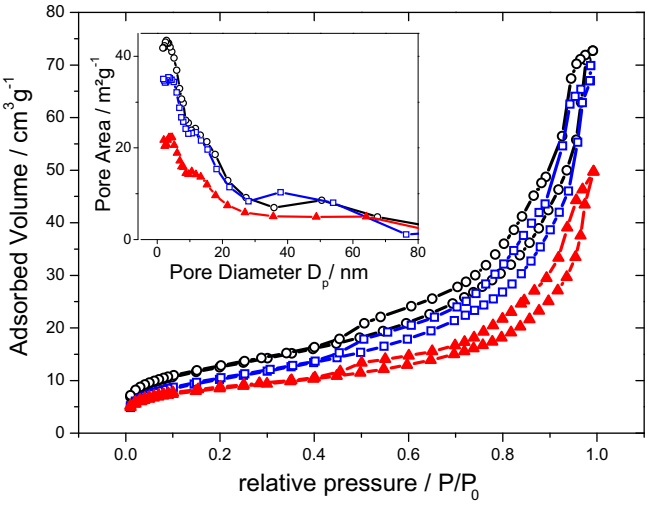

Fig. 4. Nitrogen adsorption/desorption isotherms of base porous glass 1 (–○–), grafted with $-(CH_2)_3SH$ groups 1a (–□–) and the composite glass **2a** (–▲–) obtained after complexation of $Ru(CH_3CN)_4Cl_2$. Insert: pore-size distribution from the adsorption branch of the nitrogen isotherms for **1**, **1a** and **2a**.

of pores which have non-uniform size and shape. In case of highly disordered materials like here, the desorption branch of the hysteresis loop is not necessarily correlated with the pore size [22]. Moreover, in case of highly disordered materials, BJH pore-size distribution curves obtained from the desorption branch show a spike near 4 nm which is an artefact, believed to be caused by the spontaneous evaporation of metastable pore liquid (due to the tensile strength effect). Therefore the adsorption branch was chosen for pore size analysis using the BJH method.

In base glass the micro-porosity comes according to Enke et al. [16,23] from the presence of colloidal silica formed during the preparation process of porous glasses. First, a phase separation sample with large domains of each phase is prepared at a temperature above the critical temperature. This leads to the formation of two less interconnected phases: one phase almost made of pure silica and the second one rich in boric oxide but with some silica dissolved in it. During acid leaching, the boron rich phase dissolves whereas the silica one is almost untouched. Small silica particles originating from the boron rich phase are then dispersed inside the main silica framework of the porous silica. Here, the microporosity is formed by the colloidal silica in the almost completely filled channels of the porous glass. This behaviour leads to a large pore-size distribution. The N_2 adsorption – desorption isotherm shown in Fig. 4 as well as the pore-size distribution (shown in inset of Fig. 4) performed for the base glasses show that these samples are in agreement with this description. Indeed, we observe for pore sizes larger than 5 nm a large pore-size distribution which is the sign of highly disordered materials. The specific surface area calculated using BET method is equal to 42 m^2/g, for a specific pore volume of 0.11 $m^3\,g^{-1}$ (see Table 2). From the *t*-plot calculation, the contribution of the micro-porosity to the total surface is of *ca.* 4 m^2/g, i.e. <10% which is consistent to the literature [16].

3.1.2. Functionalized hybrid glass

Grafting of the organic functionalities into the glass pores was performed by refluxing in toluene in presence of the following organic precursors $(CH_3O)_3Si(CH_2)_2SH$ (**a**), $(CH_3O)_3Si(CH_2)_2C_5H_4N$ (**b**), $(CH_3O)_3Si(CH_2)_2NH_2$ (**c**), $(CH_3O)_3Si(CH_2)_2CN$ (**d**), $(CH_3O)_3Si(CH_2)_2acac$ (**e**) (Fig. 1). In this process, the organic molecules containing the specific functional groups are covalently attached to the glass matrix *via* silylization process where a silica surface interacts with the silane reagent to form a covalent bond. The introduction of organic functional groups on the surface leads to the formation of organophilic properties to the porous glass matrix. Hybrid glasses **1a**–**e** were obtained. The organic groups contents were determined by elemental analysis for all hybrid glasses except **1e**, for which the analysis was difficult due to the presence of only C, O and H. The molar ratios of these hybrid glasses as inferred from elemental analyses are given Table 1. The surface properties of silica materials

and especially of porous glasses, which are strongly correlated with the grafting capacity, depend on the presence of silanol groups on the surface. A silanol group can be isolated (free silanol groups), with the surface silicon atom having three bonds into the bulk structure and the fourth one to OH group. It can also be vicinal or bridged when two isolated silanol groups attached to two different silicon atoms are bridged by H-bond. A third type of silanol called geminal consists of two hydroxyl groups attached to one silicon atom. The geminal silanols are close enough to form H-bond whereas free silanols are too far. Nowadays many studies based on theoretical calculations, physical and chemical methods are explored to quantify the number of silanol [21]. According to the literature, it seems that the order of magnitude of the silanol number should be independent of the origin and structural characteristics of amorphous silica and should be a physico-chemical constant. The estimated number of OH groups on the porous silica surface is between 4 and 5 OH groups per nm [24] Indeed, Zhuravlev [24] proposed a model based on a large review of the literature, which is able to predict the concentrations of the different types of OH groups as a function of the pretreatment temperature. Concerning the free silanol number, which should be key parameter to estimate the grafting capacity; it does not exceed 2 OH per nm^2 according to this review and its model, and is estimated to be about 1.2 OH per nm^2 for samples with any pretreatment temperature.

One can thus assume that in our case the concentration of free sites for grafting, i.e. the free OH group, is in the range of 1.2–2 sites per nm^2. This means that for a molecular weight of the materials of 60 g/mol and a specific surface area of 42 $m^2\ g^{-1}$, there are about 0.084–0.139 mmoles of free sites per gram of material. Considering Table 1, it is then reasonable to affirm that for all the considered functional groups (samples **1a–d**), the whole grafting capacity is used, the organic loading being in the same order than the available free sites.

The porous texture of the hybrid-functionalized glass samples (**1a–e**) was proved by nitrogen physisorption isotherm method and compared to the base glasses, as shown in Fig. 4. The shape of the physisorption curve is the same as a typical adsorption – desorption isotherm of type IV with a H2 hysteresis loop. A decrease of the specific surface area was observed for each grafted glass (see Table 2), for instance from 42 m^2/g to 33 m^2/g for **1a**, and decrease of the cumulated pore volume, for instance from 0.11 cm^3/g before to 0.09 cm^3/g for **1c**. These facts are in agreement with the presence of the organic groups into the pores of the glasses.

Transmission electron microscopy (TEM) and scanning electron microscopy (SEM) were performed on the hybrid glasses **1a–e**. The SEM and TEM images of the hybrid glass **1a** are shown Fig. 5 as an example. The porosity of the glass is clearly visible on both images with pore sizes of several tenth of nm which substantiate the results of the nitrogen physisorption analysis.

3.2. Ruthenium complexes extractions and characterisation of $Ru(CH_3CN)_4Cl_2/HS(CH_2)_2SiO_{1.5}/SiO_2–Na_2O$ composite

The second step of our approach consists in the selective extraction of the Ru species from aqueous solutions by functionalized hybrid glasses **1a–e** and characterisation of the so-obtained Ru-containing composite glasses. In this study, two precursors with different redox (acronym named reduction/oxidation) states have been tested: $[Ru^{IV}(NO_3)_3(NO)]$ and $[Ru^{II}(CH_3CN)_4Cl_2]$ with the Ru redox states of +IV and +II, respectively (see Section 2). The initially colorless hybrid glasses became brown, as it can be seen in the photograph of monolith **2a** (Fig. 6). Table 3 presents the amounts of Ru obtained by elemental analysis after extraction of $[Ru^{II}(CH_3CN)_4Cl_2]$ for all hybrid glasses. The highest amount of inserted ruthenium (0.56 wt.% corresponding to 1.86 wt.% of $[Ru^{II}(CH_3CN)_4Cl_2]$) was obtained for the hybrid glass **1a**, leading to the material **2a**.

Hybrid glasses **1b–e** also extract $[Ru^{II}(CH_3CN)_4Cl_2]$ but to a lower extent. This fact may be explained by the best complexation of the soft Ru ion by the soft thiol ligand in comparison with the other hardest ligands. The presence of covalent interactions between Ru and thiol groups is also supported by the fact that re-suspension of this composite material in water did not lead to a decrease of the amount of inserted Ru-containing complexes. Increasing the concentration of complexes or repeating the complex extraction twice did not increase the amount of inserted ruthenium. Taking into account that hybrid glass **1a** seems to be the most encouraging in order to extract $[Ru^{II}(CH_3CN)_4Cl_2]$, we performed selectivity test by using a mixture of aqueous solutions of $[Ru^{II}(CH_3CN)_4Cl_2]$ and

Fig. 6. Photographs of samples 2a and **4a**.

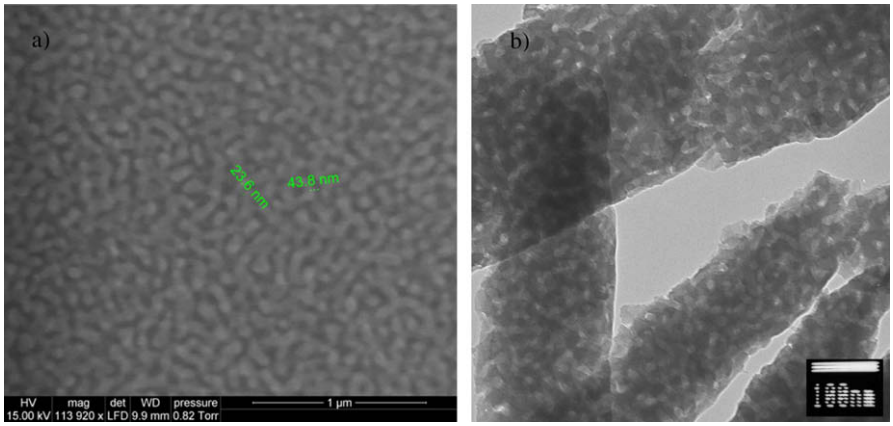

Fig. 5. SEM (a) and TEM (b) micrographs for sample **1a**.

$ErCl_3$. On the basis of the elemental analysis, no erbium ion was extracted from the solution while the typical amount of Ru (0.51 wt.%) was incorporated in the hybrid glass. In comparison with $[Ru^{II}(CH_3CN)_4Cl_2]$, $[Ru^{IV}(NO_3)_3(NO)]$ is only poorly extracted by the hybrid glasses with Ru contents in glasses smaller than 0.05 wt.% in all cases.

The composite material **2a** obtained after insertion of $[Ru^{II}(CH_3CN)_4Cl_2]$ was characterized by nitrogen physisorption, TEM and IR analyses. The N_2 adsorption–desorption isotherm curves for **2a** are compared with the porous base glass **1** and the hybrid glass **1a** before Ru complex incorporation in Fig. 4. No change in the isotherm type is observed in **2a** after incorporation of the Ru-containing complexes into the hybrid glass **1a**, which proves the conservation of the bottle-like pore system. The specific surface decreases from 35 m^2/g (for **1a**) to 24 m^2/g (for **2a**) and the cumulated pore volume from 0.10 cm^3/g (for **1a**) to 0.08 cm^3/g (for **2a**). These decreases indicate the presence of $[Ru^{II}(CH_3CN)_4Cl_2]$ in the glass pores. However, micro and mesoporosities can still be found, which again proves the preservation of the porous host structure and leads to the conclusion that the Ru complexes are located inside the pores.

TEM substantiates the results of nitrogen physisorption analyses. The TEM micrographs performed for the host structure after the complex incorporation **2a** (Fig. 7) indicate that the porous structure of the parent materials are still retained after the complex incorporation. No visible particles or bulk materials separated out of the surface of pores were observed confirming the presence of the complex exclusively in the channels. A distinctive signal for ruthenium is detected by energy dispersive spectroscopy (EDS) analysis with an atomic ratio Ru/Si of 0.55/99.45 which is in rather agreement with the Ru and Si content obtained from elemental analysis.

4. Synthesis and characterisation of RuO_2/SiO_2–Na_2O–B_2O_3 nanocomposites

The third step of our approach consists in the intrapore formation of RuO_2 nanoparticles by the thermolysis of the $[Ru^{II}(CH_3CN)_4Cl_2]$ complex anchored into the pores (Fig. 1). The thermogravimetric analysis curves of **2a,** done in air (Fig. 8) show two

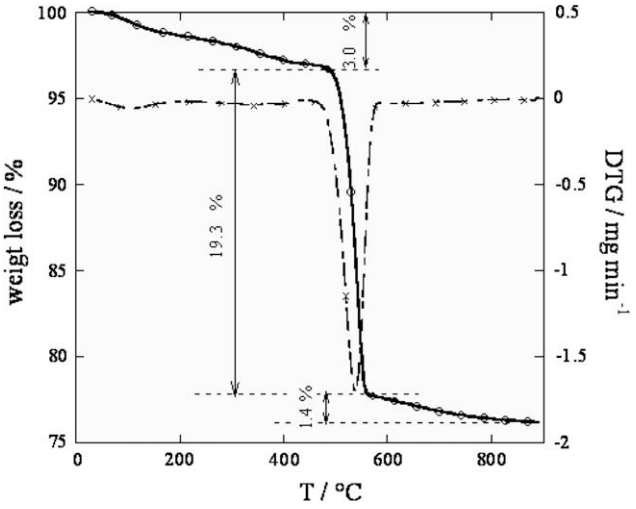

Fig. 8. TGA (–○–) and DTA (–×–) curves of **1a** under air.

weight loss steps with inflexion points at 454 and 560 °C. A first weight loss from 0.6% (105 °C) to 3% (up to 454 °C) can be attributed to the loss of water or solvent molecules that were weakly adsorbed onto the glass surface. The second weight loss of 19.3% (around 560 °C) corresponds to the elimination of organic moieties and the final transformation of the Ru complex into ruthenium oxide. At 800 °C, all organic moieties were removed and no essential change in the weight was observed up to 900 °C.

In this respect, the growth of the nanoparticles was performed by the calcination of **2a** at 650 °C in air to give **4a**. This heat treatment of **2a** leads to the formation of a blue glass sample (Fig. 6). The ruthenium content in this nanocomposite **4a** was determined by elemental analysis and is equal to 0.68 wt.% that corresponds to 0.90 wt.% of RuO_2.

Fig. 9 depicts a TEM image of the host structure with incorporated nanoparticles of RuO_2. The organisation of the host and the pore structure were clearly damaged during the heating process and no pore can be seen from TEM. On the other hand, no external

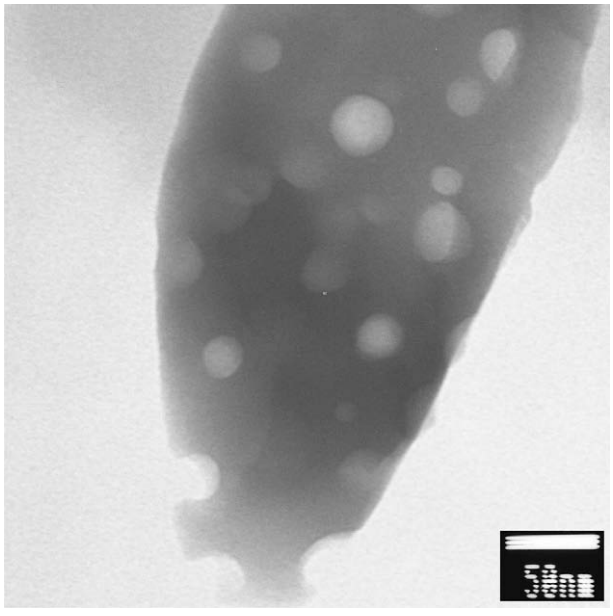

Fig. 7. TEM micrograph for sample 2a.

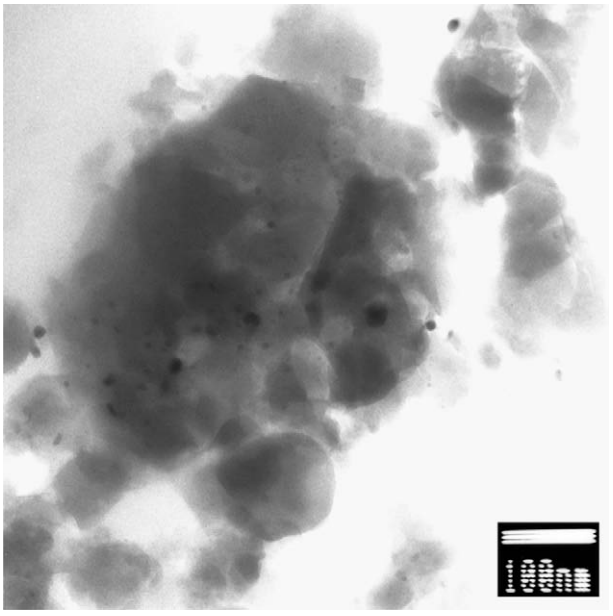

Fig. 9. TEM micrograph of glass sample 4a obtained after calcination of **2a** under air.

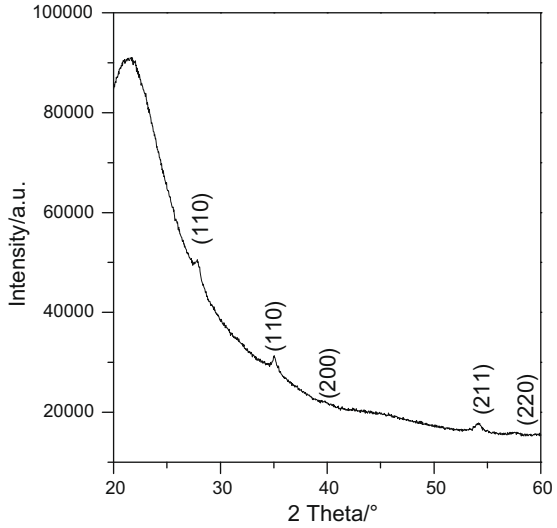

Fig. 10. XRD pattern of material **4**.

bulk ruthenium oxide phase was observed. The TEM micrographs of sample **4a** clearly show the presence of nanoparticles with a relatively narrow size distribution inside the glass. The mean size of these nanoparticles in **4a** could be estimated between 10 nm and 20 nm (Fig. 9). Obviously, the calcination of the ruthenium complex inside the porous hybrid glass precluded further growth of the RuO_2 nanoparticles and closed the glasses pores which allowed to confine the nanoparticles within the host.

Powder X-ray diffractogram of **4a** has been performed (Fig. 10). As expected for nanoparticle-containing samples, all XRD peaks are rather broad. Superposed on of the broad peak assigned to the matrix at 21.4°, the XRD profile of sample **4a** correspond to the profile of the tetragonal phase of the RuO_2 structure (PDF 40-1290). The peaks at 28.0°, 35.1° and 54° corresponding to the (1 1 0), (1 0 1) and (2 1 1) reflections have been deconvoluted to Lorentzian curves for the determination of the full-width at half maximum (FWHM) value. The crystalline domain size has been calculated from the Debye–Scherrer formula, using the FWHM value of the respective index peaks and giving values in the range of 7–15 nm.

5. Conclusion

A porous glass is produced from a borosilicate melt of an appropriate composition which exhibits spinodal decomposition into a silicate-rich glass phase and a borate glass phase after solidification. The latter phase is removed by chemical etching leaving a glass with a bicontinuous pore structure. Ruthenium complexes supported on SiO_2 nanocomposites are prepared from this mesoporous glass by subsequent grafting of an organic functional group and a ruthenium precursor. The optimum Ru immobilization was observed for the couple $HS(CH_2)_3Si(OCH_3)_3/Ru(CH_3CN)_4Cl_2$. A further heat treatment at 650 °C in air gives RuO_2-silica glass composite.

This experimental approach devoted to the design of functionalized ordered mesoporous silica-based materials is very attractive for ruthenium immobilization in High Level radioactive liquid Waste (HLW) as it allows both the separation of Ru and to some extent its confinement by applying a thermal treatment which converts the Ru complexes in RuO_2 nanoparticles and simultaneously closes the porosity of the glass matrix.

Acknowledgements

The authors thank the Centre National de Recherche Scientifique, the University of Montpellier II, the Commissariat à l'Energie Atomique and the French Research Group MATINEX (CNRS/CEA/AREVA/EDF) for their financial support.

References

[1] C. Ronneau, J. Cara, A. Rimskikorsakov, J. Environ. Radioactiv. 26 (1995) 63.
[2] R. Pflieger, M. Malki, Y. Guari, J. Larionova, A. Grandjean, J. Am. Ceram. Soc. 92 (2009) 560.
[3] K. Uruga, K. Sawada, Y. Arita, Y. Enokida, I. Yamamoto, J. Nucl. Sci. Technol. 44 (2007) 1024.
[4] H.D. Schreiber, J. Non-Cryst. Solids 84 (1986) 129.
[5] H.D. Schreiber, A.L. Hockman, J. Am. Ceram. Soc. 70 (1987) 591.
[6] H.D. Schreiber, F.A. Settle, P.L. Jamison, J.P. Eckenrode, G.W. Headley, J. Less-Common Metals 115 (1986) 145.
[7] M.A. El-Absy, M.A. El-Amir, M. Mostafa, A.A. Abdel Fattah, H.M. Aly, J. Radioanal. Nucl. Chem. 266 (2005) 295.
[8] M.A. El-Absy, H.F. Aly, M.A. Mousa, M. Mostafa, J. Radioanal. Nucl. Chem. 261 (2004) 163.
[9] J.N. Mathur, M.S. Murali, P.R. Natarajan, L.P. Badheka, A. Banerji, Talanta 39 (1992) 493.
[10] M.V.B. Krishna, J. Arunachalam, D.R. Prabhu, V.K. Manchanda, S. Kumar, Sep. Sci. Technol. 40 (2005) 1313.
[11] S.H. Lee, H. Chung, Sep. Sci. Technol. 38 (2003) 3459.
[12] R. Gandon, D. Boust, O. Bedue, Radiochim. Acta 61 (1993) 41.
[13] N.L. Sonar, P.K. Mishra, S.G. Kore, M.S. Sonavane, Y. Kulkarni, K. Raj, V.K. Manchanda, Sep. Sci. Technol. 44 (2009) 506.
[14] K. McEleney, D.P. Allen, A.E. Holliday, C.M. Crudden, Org. Lett. 8 (2006) 2663.
[15] X.S. Li, A.R. Courtney, W. Yantasee, S.V. Mattigod, G.E. Fryxell, Inorg. Chem. Commun. 9 (2006) 293.
[16] D. Enke, F. Janowski, W. Schwieger, Micropor. Mesopor. Mat. 60 (2003) 19.
[17] A.S. Tkachev, T.V. Antropova, V.P. Veiko, I.A. Drozdova, Glass Phys. Chem. 30 (2004) 173.
[18] G. Clavel, Y. Guari, J. Larionova, C. Guerin, New J. Chem. 29 (2005) 275.
[19] V. Matsura, Y. Guari, J. Larionova, C. Guerin, A. Caneschi, C. Sangregorio, E. Lancelle-Beltran, A. Mehdi, R.J.P. Corriu, J. Mater. Chem. 14 (2004) 3026.
[20] B. Folch, Y. Guari, J. Larionova, C. Luna, C. Sangregorio, C. Innocenti, A. Caneschi, C. Guerin, New J. Chem. 32 (2008) 2299.
[21] B.F.G. Johnson, J. Lewis, I.E. Ryder, J. Chem. Soc. Dalton Transac. (1977) 719.
[22] S. Lowell, J.E. Shields, M.A. Thomas, M. Thommes, Characterization of Porous Solids and Powders: Surface Area, Pore Size and Density, Springer, 2006.
[23] D. Enke, K. Otto, F. Janowski, W. Heyer, W. Schwieger, W. Gille, J. Mater. Sci. 36 (2001) 2349.
[24] L.T. Zhuravlev, Colloids Surf. Physicochem. Eng. Aspects 173 (2000) 1.